EEET ECOLOGICAL ENGINEERING & ENVIRONMENTAL TECHNOLOGY

Ecological Engineering & Environmental Technology, 2026, 27(8), 87–103
https://doi.org/10.12912/27197050/224860
ISSN 2719–7050, License CC-BY 4.0

Received: 2026.06.20
Accepted: 2026.07.10
Published: 2026.08.01

Evaluation of a conical insert for improving fertilizer distribution uniformity in a centrifugal spreader

Nacera Siakhene Hennouni[1*], Mohamed Amine Hennouni[2], Sameh Messaoudi[1], Charfeddine Zekri[3]

[1] Laboratoire Biodiversité et Pollution des Écosystèmes, Faculté des Sciences de la Nature et de la Vie (SNV), Université Chadli Bendjedid El Tarf, 36000 El Tarf, Algeria
[2] Laboratoire des Ressources Naturelles et Aménagement des Milieux Sensibles (RNAMS), Université Larbi Ben M'Hidi, Oum El Bouaghi, Algeria
[3] Department of Mechanical and Agro-Industrial Engineering, Higher School of Engineers of Medjez el Bab, University of Jendouba, Medjez el Bab, Tunisia
* Corresponding author's e-mail: hennouni-nacera@univ-eltarf.dz

ABSTRACT

A quarter-scale laboratory prototype of a centrifugal fertilizer spreader was evaluated to determine whether a conical flow-guiding insert could improve the transverse distribution of granular fertilizer. Experiments were conducted at the Department of Mechanical and Agro-Industrial Engineering, Higher School of Engineers of Medjez el Bab, Tunisia. The methodology combined indoor spreading tests with three replicates per treatment, particle-size classification, and reduced-order semi-empirical modeling. The prototype was equipped with a 19 cm inclined disc, three vanes, and a conical insert with four longitudinal channels and a 12 mm discharge opening. Transverse profiles were measured from -5 to +5 m without the insert at 779 rpm and with the insert at 708, 779, and 816 rpm, using a fertilizer flow rate of 4.2 kg min^{-1}. Additional half-profile measurements were collected for three particle-size classes of 2.00, 1.25, and 1.00 mm. The conical insert reduced the coefficient of variation from 68.2% without an insert to 12.0% at 779 rpm with an insert, indicating a marked improvement in transverse uniformity. The best insert configuration was observed at 779 rpm, whereas 708 and 816 rpm produced higher variability. Particle-size analysis showed that the 1.25 mm fraction produced the most uniform half-profile, while 1.00 mm particles were concentrated near the center and 2.00 mm particles contributed more strongly to distant positions. Because an initial physics-based model did not adequately reproduce the measured profiles, the final modeling strategy used parsimonious semi-empirical functions selected by the corrected Akaike information criterion and evaluated by leave-one-out cross-validation. This approach provided a transparent framework for comparing configurations and documenting the effects of rotational speed and particle diameter.

Keywords: centrifugal fertilizer spreader, conical insert, fertilizer distribution, particle size, semi-empirical model, indoor experiment.

INTRODUCTION

Degradation of agricultural soils caused by nutrient depletion, wildfire impacts, erosion, salinization, climate-related stress, and contamination by potentially toxic elements has become a major environmental challenge (Wuyep et al., 2024; Odiana et al., 2026; Wuyep et al., 2026). Restoration and soil-quality improvement strategies increasingly rely on the application of soil amendments and agronomic inputs such as mineral fertilizers, organic residues, moisture-retaining materials, and other soil-management practices (Patah and Othman, 2024; Sikder and Mumit, 2024; Khokhar et al., 2025). Numerous studies have focused on identifying effective amendment materials and evaluating their influence on soil fertility, nutrient availability, water retention, crop performance, and ecosystem resilience (Sikder and Mumit, 2024; Khokhar et al., 2025;

Wuyep et al., 2026). However, substantially less attention has been devoted to the engineering aspects of amendment delivery, despite the fact that the effectiveness of any soil amendment depends not only on its intrinsic properties but also on its spatial distribution within the field. Non-uniform application may create localized zones of amendment accumulation and deficiency, reducing agronomic efficiency, increasing costs, and limiting the expected environmental benefits of soil restoration practices. This issue is particularly relevant for granular materials such as fertilizers, biochar granules, liming products, and remediation amendments that are commonly distributed using centrifugal spreaders.

Achieving accurate and uniform fertilizer distribution is a central agronomic objective that directly affects crop yield, input efficiency and environmental impact. Non-uniform spatial distribution of granular fertilizer leads to local over-fertilization, increased nitrogen and phosphorus losses, and reduced economic return (Villette et al., 2017). Among the available application technologies, centrifugal disc spreaders remain widely used by farmers because of their low operating cost, ease of maintenance, and large working width, which can reach several tens of meters under field conditions (Liedekerke et al., 2009). However, the uniformity of their distribution pattern can deteriorate when application rate, feed position, disc speed, vane configuration, or fertilizer physical properties are not well controlled (Guan et al., 2022; Kömekçi et al., 2024; Juodišius et al., 2025). The spreading process in a centrifugal spreader begins with the gravitational flow of fertilizer particles from the hopper toward the rotating disc, where the vanes accelerate the granules before ejection. The initial position of particles on the disc is governed by the geometry of the discharge opening, the flow rate, and the presence or absence of flow-guiding elements. The uniformity of the resulting distribution is commonly assessed from the transverse distribution pattern and its coefficient of variation, which remains a standard criterion in recent studies on fertilizer spreader performance (Cieniawska and Pentoś, 2024). A Gaussian-shaped profile centered on the spreader centerline generally allows good uniformity by overlapping successive passes, whereas asymmetrical or multi-modal profiles produce unacceptable spatial variability.

The mechanical design of the discharge zone and the hopper outlet has therefore received increasing attention as a practical lever for improving spreading quality. Several studies have explored insert geometries, feed gate shapes, and cone-disc configurations to modify the initial distribution of particles on the disc and to reduce the sensitivity of the spreading pattern to flow-rate variations (Kweon and Grift, 2006; Liu et al., 2018; Lu et al., 2016). Conical inserts positioned at the hopper outlet may provide a low-cost mechanical solution capable of redistributing the particle flow before disc contact. However, the effect of such inserts remains insufficiently quantified under controlled experimental conditions that separate the geometrical effect of the insert from the influence of disc speed and particle size.

Granulometric composition is another factor that affects spreading uniformity in centrifugal spreaders. Larger particles generally have higher inertia and may be projected farther from the spreader, whereas smaller particles are more sensitive to aerodynamic drag, segregation, and local contact conditions on the spreading disc (Antille et al., 2015; Juodišius et al., 2025). This size-dependent behavior implies that polydisperse fertilizers can exhibit complex transverse profiles even under nominally identical operational settings. Characterizing the spatial distribution of each granulometric class separately is therefore important for understanding the contribution of particle diameter to overall spreading heterogeneity.

Mathematical modeling has been widely used to support the experimental investigation of centrifugal spreaders. Mechanistic models based on particle trajectory equations have been developed by Olieslagers et al. (1996), Dintwa et al. (2004), and Villette et al. (2005), and extended to discrete element simulations by Liedekerke et al. (2006, 2009) and Coetzee and Lombard (2011). These models provide valuable mechanistic insight when disc geometry, vane configuration, and particle properties are precisely known. In contrast, reduced-order semi-empirical models provide a simpler alternative by describing measured profiles with parsimonious mathematical functions while controlling model complexity through objective criteria such as the corrected Akaike information criterion. Recent studies on granular-material spreaders confirm the relevance of simplified mathematical modeling and simulation-based optimization for describing distribution patterns and improving spreader design (Nukeshev et al., 2023; Ou et al., 2025).

Despite the growing body of work on centrifugal spreader design, a critical gap remains: the isolated mechanical effect of a fixed conical flow-guiding insert placed at the hopper outlet has not been sufficiently quantified under controlled conditions while accounting for the influence of disc speed and particle diameter. Most previous studies have focused either on theoretical trajectory modeling or on commercial spreading configurations without specifically isolating the contribution of a single passive flow-guiding element installed before particle contact with the rotating disc. In particular, there is a lack of studies that simultaneously evaluate (i) the effect of a conical insert on profile uniformity, (ii) the interaction between insert performance and disc rotational speed, and (iii) the contribution of different particle-size fractions to the resulting spreading pattern under identical operating conditions.

Therefore, the present study addressed this gap by providing, to the authors' knowledge, controlled experimental evidence of the effect of a conical insert with four longitudinal channels on the transverse spreading profile of a quarter-scale centrifugal fertilizer spreader prototype. The central scientific hypothesis was that positioning a conical insert immediately above the discharge zone redistributes the granular flow before disc contact, thereby reducing the central concentration observed in the no-insert configuration and producing a flatter, more uniform transverse distribution. It was further hypothesized that this effect is non-linear with respect to rotational speed, and that different particle-size classes respond differently to the insert because of inertia-driven separation during particle acceleration and projection.

The new result sought in this work was the quantitative assessment of the improvement in distribution uniformity associated with the installation of the conical insert, expressed by changes in the coefficient of variation of the transverse particle-count profile. The study also aimed to identify the rotational speed at which this improvement is maximized and to determine how particle-size class affects the spatial distribution pattern under the insert configuration. By combining indoor spreading experiments, granulometric characterization, and a reduced-order semi-empirical modeling framework, this work established a transparent experimental and modeling basis for evaluating conical inserts as low-cost mechanical devices for improving fertilizer application quality and reducing spatial heterogeneity during granular amendment delivery.

MATERIALS AND METHODS

Methodological approach

This study combined controlled indoor spreading experiments, granulometric characterization and reduced-order semi-empirical modeling. All experiments were conducted at the Department of Mechanical and Agro-Industrial Engineering, Higher School of Engineers of Medjez el Bab, University of Jendouba, Tunisia. The prototype was constructed at one-quarter the linear scale of a commercial centrifugal spreader, which allowed controlled indoor testing while preserving the main geometrical relationships governing particle delivery to the disc.

The experimental component provided the primary evidence for comparing spreading behavior with and without the conical insert. The modeling component was used only to describe the measured profiles using simple mathematical functions and to quantify goodness of fit through objective indicators. This strategy was adopted because the first purely physics-based representation did not sufficiently reproduce the experimental profiles. Accordingly, the final model was treated as a calibrated reduced-order semi-empirical model rather than a full predictive mechanical simulation.

The complete workflow included prototype preparation, insert mounting, fertilizer classification by particle size, indoor spreading tests, particle counting along the transverse measurement axis, semi-empirical model fitting, model selection by corrected Akaike information criterion, and validation by leave-one-out cross-validation.

Experimental centrifugal spreader

The spreading tests were carried out using a quarter-scale centrifugal fertilizer spreader prototype designed and fabricated at the Department of Mechanical and Agro-Industrial Engineering, Higher School of Engineers of Medjez el Bab. The prototype consisted of a hopper, a discharge opening, a conical insert, a rotating disc, three vanes, an electric motor, and a supporting frame, reproducing the main functional stages of a conventional centrifugal spreader: gravitational feeding, discharge regulation, particle acceleration, and projection toward the receiving area (Figure 1).

The rotating disc had a diameter of 19 cm and was inclined by 10 degrees relative to the horizontal plane. The disc was equipped with three vanes arranged symmetrically around the rotation axis, each of length 8 cm and positioned approximately 2 cm from the disc center. The disc was driven by an electric motor, and the rotational speed was adjusted according to each experimental configuration. The spreader was mounted on a rigid mobile frame, and the discharge height was maintained at 0.70 m above the reception plane during all tests. All experiments were performed indoors on a flat concrete surface to minimize the influence of wind, ground roughness, and environmental variability.

Conical insert

The main mechanical modification evaluated in this study was a conical insert placed inside the hopper immediately above the discharge zone (Figure 2). The role of the insert was to regulate the fertilizer flow before particle

Figure 1. Quarter-scale centrifugal fertilizer spreading prototype fabricated at the Department of Mechanicaland Agro-Industrial Engineering, Higher School of Engineers of Medjez El Bab. General view showing the hopper, supporting frame, motorized rotating disc, and experimental mounting system used during the indoor spreading tests

contact with the rotating disc. Without the insert, particles were discharged mainly toward the central region of the disc. With the insert, the flow was redistributed before reaching the disc, modifying the initial particle positions and thus the transverse spreading pattern.

The conical insert had a measured base diameter of 120 mm and a cone angle of 38°. Its lateral surface included four longitudinal channels uniformly distributed at 90° intervals. Each channel had a width of 10 mm and an effective length of 90 mm. Two channel-section depths were considered: C1 = 5 mm and C2 = 15 mm, depending on the profiled section of the insert. The discharge opening was adjusted and fixed at 12 mm for all experiments involving the insert. A dimensional schematic of the insert, including A, B, C1, C2, D, H, and α, is provided in Figure 2. In the experimental interpretation and modeling workflow, the insert was considered as a mechanical flow-guiding component the effect of which was evaluated through the measured spreading profiles.

Fertilizer material and granulometric analysis

The spreading material used in the experiments was a granular mineral fertilizer with generally spherical to sub-spherical particles, making it suitable for controlled centrifugal spreading tests. Since fertilizer distribution is strongly affected by particle size, the material was characterized by sieve analysis before the spreading experiments.

Fertilizer particles were separated into three nominal granulometric classes using mechanical sieving. The retained classes were D1 = 2.00 mm, D2 = 1.25 mm and D3 = 1.00 mm. These classes were selected because particle diameter affects interaction with the rotating disc, projection distance, and final spatial distribution. Larger particles generally have higher inertia and may reach greater distances, whereas smaller particles are more sensitive to drag and local perturbations (Antille et al., 2015; Liedekerke et al., 2009). The sieving operation is shown in Figure 3.

Color marking of particle classes

To facilitate visual identification and counting after spreading, the three granulometric classes were marked using distinct food-grade colors. The coloring process was applied uniformly within each granulometric class to ensure consistent visual contrast. Minimal

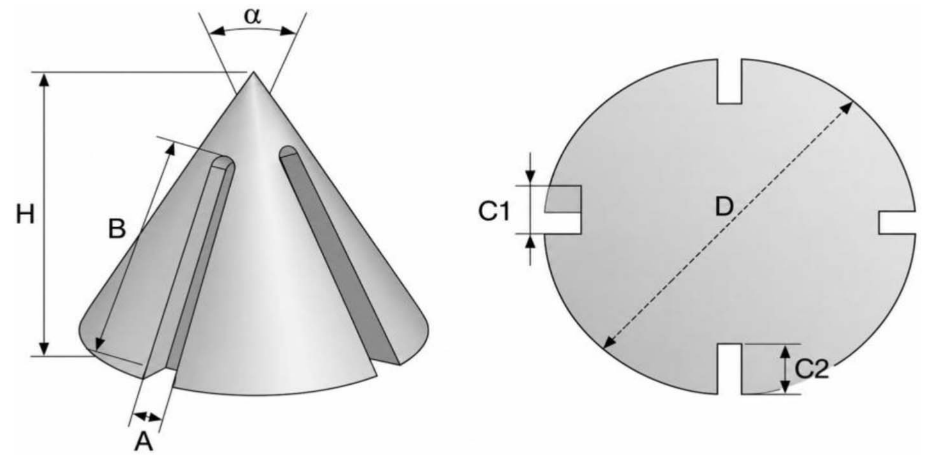

Figure 2. Geometry and dimensional schematic of the conical insert. The figure shows the three-dimensional conical body, the four longitudinal flow-guiding channels, and the main geometric parameters used for reproducibility, including channel width (A), channel length (B), channel depths (C1 and C2), cone diameter (D), cone height (H), and cone angle (α)

Figure 3. Granulometric analysis of the fertilizer by sieving. Photograph of the sieve stack used to separate the fertilizer into different particle-size classes before the spreading experiments

dye quantities were used to avoid any visible modification of particle size distribution, particle shape, surface condition or bulk behavior. The dyed particles were allowed to dry before spreading so that no wet agglomeration or additional surface adhesion affected deposition. The coloring procedure was therefore considered to have a negligible influence on particle mass and aerodynamic behavior under the controlled laboratory conditions. This procedure allowed particles belonging to D1, D2, and D3 to be counted separately after deposition. Color marking was applied for the granulometric half-profile measured at 779 rpm with the conical insert, making it possible to analyze the spatial behavior of coarse, medium, and fine fertilizer particles separately (Figure 4).

Experimental reception area

The spreading tests were performed in an indoor experimental area. A transverse reception line was established perpendicular to the spreader centerline. The reception area consisted of individual square collection trays measuring 25 × 25 cm, positioned edge to edge along the transverse axis, perpendicular to the direction of travel of the spreading unit, in accordance with the tray-based collection layout recommended by ASABE S341 (ASABE Standards, 2015). Particle collection positions were located from -5 to +5 m relative to the centerline, with a regular spacing of 1 m between adjacent measurement points, providing 11 measurement positions for each transverse profile, with one collection tray centered on each measurement position:

$$x = [-5, -4, -3, -2, -1, 0, 1, 2, 3, 4, 5]\ m \quad (1)$$

The number of particles deposited at each position was counted and used to construct the experimental spreading profiles. Figure 5 shows the collection layout used during the indoor tests. The same spatial grid of collection trays was used for all treatments. Before each experimental run, the alignment of the reception line relative to the spreader axis was checked and adjusted if necessary, in order to keep the positioning error of the collection trays within the centerline below the nominal 1 m spacing between adjacent positions and to minimize any systematic offset between the no-insert and insert configurations.

Figure 4. Colored fertilizer particle-size classes. Colored fertilizer fractions corresponding to the three granulometric classes used in the spreading tests: D1 = 2.00 mm, D2 = 1.25 mm, and D3 = 1.00 mm

Experimental treatments

The experiments compared two main configurations: spreading without an insert and spreading with a conical insert. The no-insert configuration served as the reference condition. The insert configuration was tested at three disc rotational speeds: 708, 779, and 816 rpm. For insert treatments, the fertilizer flow rate was maintained at 4.2 kg min^{-1}. Each treatment combination was replicated three times under identical laboratory conditions. Before each replicate, the hopper was completely filled to the same initial level in order to ensure comparable starting conditions for fertilizer discharge. The discharge opening, conical insert position, and reception grid were reset to the initial configuration before each run. Between successive replicates, the reception area was fully cleaned to prevent particle carry-over.

Before fertilizer release, the disc was accelerated to the target rotational speed and allowed to stabilize for 30 s. The rotational speed was checked before each run, and fertilizer release was started only when the disc speed remained within ±5 rpm of the target value. This procedure ensured that all replicates started under comparable operating conditions and reduced variability related to hopper filling level or disc-speed fluctuation. For each replicate, particle counts at each collection position were recorded separately and then averaged across the three replicates. The mean values were used as input profiles for subsequent modeling, while the standard deviation was calculated to quantify between-replicate variability. This averaging approach assumes that intra-treatment variability is random and does not introduce systematic bias in the spatial distribution. The results shown in Table 1 provide the mean transverse particle-count profiles used to evaluate the effects of the conical insert and rotational speed on fertilizer distribution.

Granulometric spreading profiles

The effect of particle size was evaluated using half-profiles measured at 779 rpm with the conical insert. The distances considered ranged from 0 to 5 m:

$$x = [0, 1, 2, 3, 4, 5]\ m \qquad (2)$$

Each granulometric class was tested in three independent replicates under identical experimental conditions, and mean particle counts were used for analysis. The granulometric classes were separated before spreading by mechanical sieving. Each class was then tested independently in separate sequential experimental runs, with a separate hopper filling for each particle-size

Figure 5. Experimental spreading layout. Indoor experimental setup showing the centrifugal spreade and the reception area used to collect and quantify the transverse distribution of fertilizer particles

Table 1. Mean transverse particle-count profiles across three replicates, used for model fitting and comparison

Configuration	Rotational speed (rpm)	Flow rate (kg min⁻¹)	Particle counts from -5 to +5 m
Without insert	779	4.2	6, 12, 31, 51, 63, 69, 63, 51, 31, 12, 6
With conical insert	708	4.2	22, 25, 33, 42, 52, 57, 52, 42, 33, 25, 22
With conical insert	779	4.2	41, 42, 46, 53, 53, 55, 53, 53, 46, 42, 41
With conical insert	816	4.2	33, 42, 44, 56, 58, 67, 58, 56, 44, 42, 33

Note: Values are means of three replicates. Counts are listed according to transverse coordinate x = -5, -4,..., +5 m.

Table 2. Granulometric half-profiles measured at 779 rpm with the conical insert

Particle class	Nominal diameter (mm)	Particle counts from 0 to 5 m
D1	2.00	9, 7, 8, 12, 12, 15
D2	1.25	21, 20, 20, 20, 19, 20
D3	1.00	25, 26, 25, 14, 11, 6

Note: Values are means of three replicates. Counts are listed according to half-profile coordinate x = 0, 1, 2, 3, 4, and 5 m.

class. Between successive class tests, the hopper, discharge zone, conical insert, rotating disc, and reception area were cleaned to minimize cross-contamination between granulometric classes.

Particle counts were treated as proportional to deposited mass within each granulometric class because each sieve fraction had a narrow nominal particle-size range. No independent mass-to-count calibration or verification test was performed for the colored fractions; therefore, the granulometric results were interpreted as comparative particle-count profiles rather than absolute deposited-mass measurements. The same counting method was applied consistently to all particle-size classes, allowing comparison of the relative spatial behavior of coarse, medium, and fine particles under the conical insert configuration.

The granulometric half-profiles were measured independently using a single-sided sampling configuration under conditions identical to those of the corresponding full transverse profile measurements. Table 2 presents the mean half-profiles used to assess the influence of particle diameter on spatial distribution under the conical insert configuration.

Experimental procedure

Before each test, the spreader was positioned at a fixed location relative to the reception area. The hopper, discharge system, insert, and rotating disc were inspected to ensure correct alignment. Before each run, the hopper was completely filled to the same initial level in order to maintain comparable starting conditions for fertilizer discharge. The disc was then accelerated until the target rotational speed was reached and allowed to stabilize for 30 s before fertilizer was introduced. Fertilizer release was started only when the measured rotational speed remained within ±5 rpm of the target value.

For each run, a weighed quantity of fertilizer was introduced into the hopper and allowed to flow through the discharge system. In the no-insert configuration, particles fell directly onto the rotating disc. In the insert configuration, particles were guided by the conical insert before reaching the disc. After projection, particles deposited at each collection position were counted manually. Although ASABE S341 recommends collecting and weighing fertilizer mass in standard trays, particle counting by visual identification was deliberately chosen because the quarter-scale prototype produced small per-position masses and the color marking allowed differentiation between size classes during counting. For a given pre-sieved and color-marked particle class, the number of collected particles was considered proportional to local deposited mass, because particles within each class had a narrow nominal diameter range. No independent mass-to-count calibration was performed; therefore, the particle-size results were interpreted as comparative particle-count profiles rather than absolute deposited-mass measurements. This procedure was therefore used as a scale-adapted measurement method for comparative laboratory evaluation, while acknowledging that field-scale testing should use the standard tray-mass approach.

Each treatment was replicated three times. Between successive replicates, the experimental area was cleaned carefully to remove residual particles and avoid contamination between runs. The reception trays, hopper, discharge zone, insert, and rotating disc were also checked and cleaned when necessary to prevent residual particle accumulation and cross-contamination between runs. The mean particle counts across the three replicates were used for model fitting; within-treatment standard deviation was used to compute between-replicate variability when required. All tests were performed inside a large indoor hangar on a flat concrete surface, protected from direct outdoor airflow. Therefore, wind effects were minimized in the experimental environment. Ambient air movement was checked near the spreader and along the reception line before testing, and the tests were performed only under still-air indoor conditions. The receiving surface inclination was below 2%, consistent with ASABE S341 standard conditions (ASABE Standards, 2015).

Semi-empirical reduced-order modeling

Because the initial physics-based model showed non-negligible deviations from the measured profiles, the final modeling strategy was revised toward a calibrated reduced-order semi-empirical approach. The purpose of the model was not to simulate all particle mechanics inside the spreader, but to provide a robust mathematical description of the measured profiles and to compare spreading configurations using objective indicators. The modeling workflow and raw profiles are shown in Figure 6. All model inputs were derived from the original laboratory measurements generated in this study; no data from annual reports, questionnaires, or secondary datasets were used as model inputs.

The modeling was implemented in Python using NumPy, SciPy, pandas and Matplotlib in a Google Colab notebook. The workflow included data loading, model definition, parameter estimation, model selection, cross-validation, calculation of performance indicators, and automatic figure generation.

To ensure computational reproducibility, the complete modeling workflow was kept in a single executable notebook, using the same input tables provided in the Supplementary Materials. No stochastic simulation procedure was used in the final semi-empirical model; therefore, the fitted parameters and performance indicators are reproducible when the notebook is executed with the same raw input data. The notebook and calculation outputs were archived together with the supplementary dataset to allow independent verification of the modeling workflow.

Main profile model

The main model used to describe each full transverse profile was a Gaussian function with a constant baseline:

$$N(x) = C + A\,exp[-x^2 / (2\sigma^2)] \quad (3)$$

where: $N(x)$ is the predicted number of particles at distance x, C is the baseline level, A is the central amplitude, and σ is the dispersion parameter. This model was selected because it is parsimonious and interpretable: C represents the lateral deposition level, A the central concentration, and σ the spreading width.

The background-plus-Gaussian model was defined a priori as the main candidate model for

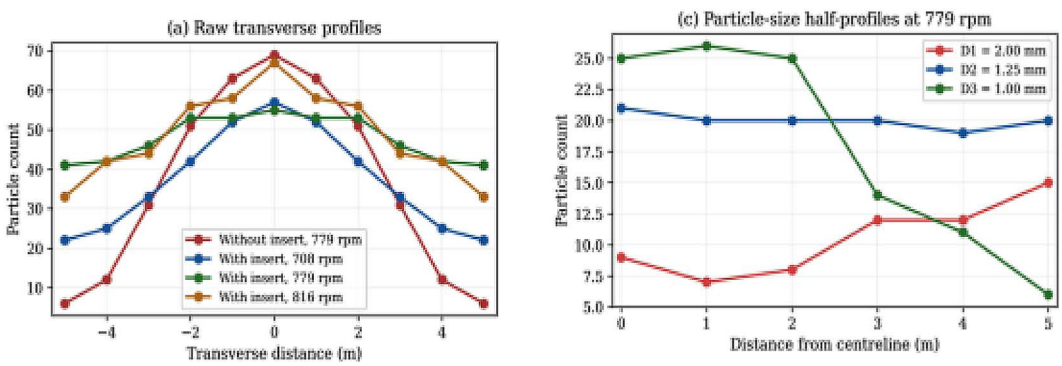

Figure 6. Semi-empirical modeling workflow and raw transverse profiles. The figure summarizes the experimental profiles used for model fitting and comparison

the full transverse profiles. This choice was based on the fact that transverse spreading patterns from broadcast and centrifugal spreaders are commonly represented using bell-shaped or normal-distribution-based functions (Grift, 2000; Villette et al., 2017), because these functions provide a simple and interpretable description of central deposition and lateral decay. In the present model, the constant baseline represented residual lateral deposition, whereas the Gaussian component described the central concentration and spreading width. The suitability of this a priori candidate model was then evaluated against alternative candidate functions using AICc and model-performance indicators. Therefore, the final use of the background-plus-Gaussian model was based on both physical interpretability and comparative model selection. A lower central amplitude combined with a higher baseline indicates a more laterally redistributed profile.

Alternative candidate models

To avoid relying on a single arbitrary model form, several candidate models were considered. Depending on the data subset, these included linear, quadratic, Gaussian, and exponential-type functions. The general polynomial form was:

$$N(x) = \beta_0 + \beta_1 x + \beta_2 x^2 + \varepsilon \tag{4}$$

where: β_0, β_1, and β_2 are fitted coefficients and ε is the residual error. For granulometric half-profiles, linear, quadratic, and exponential-type models were tested when appropriate.

The final retained model was selected based on the lowest AICc value, while also considering model parsimony. When two candidate models showed comparable support, defined as an AICc difference lower than 2 (ΔAICc < 2), the simpler model with fewer fitted parameters was preferred to reduce the risk of overfitting and improve interpretability.

Parameter estimation and model selection

Model parameters were estimated by minimizing the sum of squared residuals between measured and predicted particle counts:

$$SSE = \Sigma(Ni,exp - Ni,pred)^2 \tag{5}$$

where: Ni,exp is the measured number of particles at position i, and $Ni,pred$ is the corresponding model prediction.

For nonlinear models, parameter estimation was performed using the bounded Trust Region Reflective algorithm implemented in scipy.optimize.curve_fit. Lower and upper parameter bounds were imposed during fitting to maintain physically meaningful solutions; in particular, baseline, amplitude, and dispersion parameters were constrained to non-negative values where appropriate. Negative predicted particle counts were therefore avoided through this constrained optimization procedure itself, rather than through an a posteriori correction or a penalty function applied after fitting.

Model selection was based on the corrected Akaike information criterion (AICc), which is more appropriate than AIC when the number of observations is small (Burnham and Anderson, 2002). AICc was calculated as:

$$AICc = n\,ln(SSE/n) + \\ + 2k + [2k(k + 1)] / (n - k - 1) \tag{6}$$

where: n is the number of observations, k is the number of fitted parameters, and SSE is the sum of squared errors.

The model with the lowest AICc was retained as the preferred model. When two candidate models showed comparable support, defined as an *AICc* difference lower than 2 (ΔAICc < 2), the simpler model with fewer fitted parameters was preferred to reduce the risk of overfitting and improve interpretability.

Leave-one-out cross-validation and indicators

Model robustness was evaluated using leave-one-out cross-validation. In this procedure, one observation was removed from the dataset, the model was fitted using the remaining observations, and the omitted point was predicted. This process was repeated until every observation had been omitted once. For each leave-one-out iteration, parameter estimation was repeated using only the training subset, and the omitted observation was not used during model fitting. The same bounded Trust Region Reflective algorithm and parameter bounds used for the full-dataset fit were applied at every leave-one-out iteration, so that negative predicted particle counts were prevented identically during cross-validation and during the main model fit. The leave-one-out prediction error was used to evaluate whether the model depended excessively on any individual point. The coefficient of variation was used to quantify spreading heterogeneity:

$$CV(\%) = (sN / \bar{N}) \times 100 \quad (7)$$

where: sN is the standard deviation of particle counts, and $\bar{N}$ is the mean particle count.

For transverse profiles, CV was calculated from the spatial distribution of particle counts across measurement positions and was therefore used as an indicator of spreading uniformity. Lower CV values indicate a more homogeneous transverse distribution. The coefficient of determination, root mean square error, mean absolute error, normalized root mean square error, and Willmott index were calculated as follows:

$$R^2 = 1 - SSE / SST \quad (8)$$

$$RMSE = \sqrt{[(1/n)\Sigma(Ni,exp - Ni,pred)^2]} \quad (9)$$

$$MAE = (1/n)\Sigma|Ni,exp - Ni,pred| \quad (10)$$

$$NRMSE(\%) = RMSE / (Nmax,exp - Nmin,exp) \times 100 \quad (11)$$

$$d = 1 - \Sigma(Pi - Oi)^2 / \Sigma(|Pi - \bar{O}| + |Oi - \bar{O}|)^2 \quad (12)$$

where: Oi represents the observed particle count, Pi represents the predicted particle count, $\bar{O}$ is the mean observed particle count, n is the number of observations, and Nmax,exp and Nmin,exp are the maximum and minimum experimental particle counts, respectively.

These indicators were used jointly because each describes a different aspect of model performance. R^2 indicates explained variance, RMSE and MAE quantify absolute error, NRMSE expresses error relative to the observed range, and Willmott d indicates agreement between measured and predicted values (Willmott, 1982). The combined use of these indicators avoided relying on a single goodness-of-fit criterion and allowed model performance to be assessed in terms of explained variance, prediction error, relative error, and agreement with measured data.

RESULTS

Effect of the conical insert on the transverse profile

The no-insert configuration produced a strongly peaked distribution centered on the spreader axis, with the maximum count located at x = 0 m. In contrast, the conical insert generated a flatter distribution at the same rotational speed of 779 rpm. As shown in Figure 7, the profile with the insert had lower central dominance and higher lateral deposition than the reference configuration without an insert.

The coefficient of variation decreased from 68.2% without insert to 12.0% with insert at 779 rpm (Table 3), corresponding to a reduction of 56.2 percentage points. The semi-empirical background-plus-Gaussian model fitted both profiles with high agreement, with R^2 values of 0.992 for the no-insert configuration and 0.951 for the insert configuration. The lower CV observed with the insert indicates a more homogeneous transverse distribution.

Effect of rotational speed under the insert configuration

Rotational speed affected the transverse spreading profile under the insert configuration (Figure 8). Among the three tested speeds, 779 rpm gave the lowest experimental coefficient of variation (12.0%), followed by 816 rpm (23.0%) and 708 rpm (35.1%). This indicates that the intermediate speed produced the most uniform distribution in the tested range.

The background-plus-Gaussian model was retained for all rotational speeds according to AICc (Table 3). The fit quality was high for all three insert profiles, with R^2 values of 0.999, 0.951, and 0.948 for 708, 779, and 816 rpm, respectively. The leave-one-out cross-validation RMSE ranged from 0.62 to 3.45 particles, confirming that the semi-empirical model remained robust for the transverse profiles. The fitted parameter values of C, A, and σ are provided in Supplementary File S1 (Table S1).

Effect of particle size

Particle-size class strongly influenced the half-profile measured at 779 rpm with the conical insert (Figure 9). The 1.25 mm class showed the most uniform distribution, with a CV of only 3.2%. The 2.00 mm class showed increasing counts toward greater distances, whereas the 1.00 mm class was concentrated mainly near the center and decreased sharply beyond 2 m.

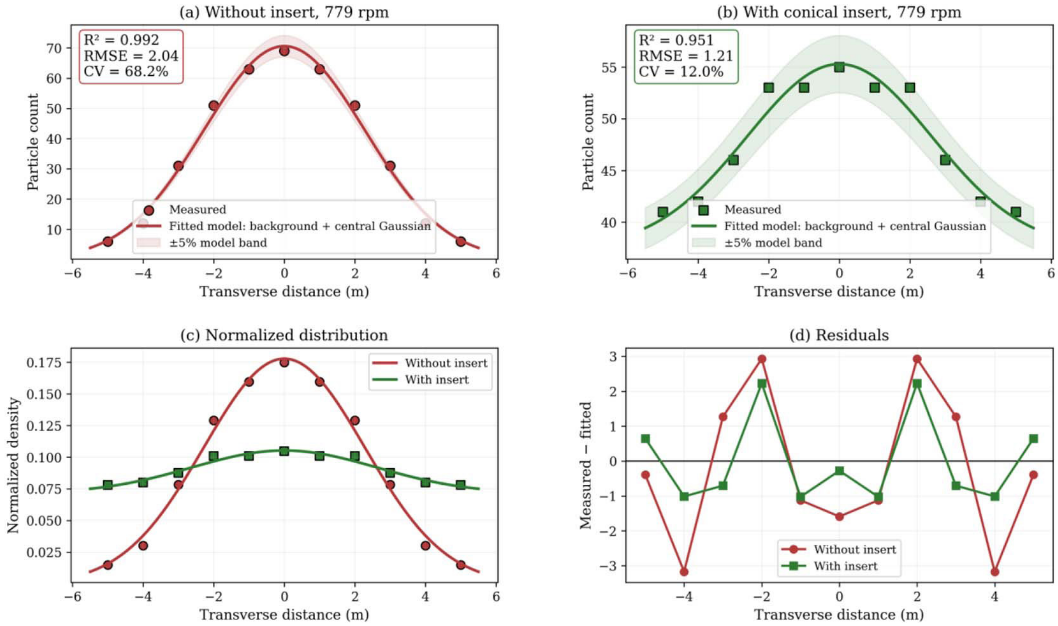

Figure 7. Effect of the conical insert on the transverse spreading profile at 779 rpm. The figure compares the measured and fitted profiles with and without the insert

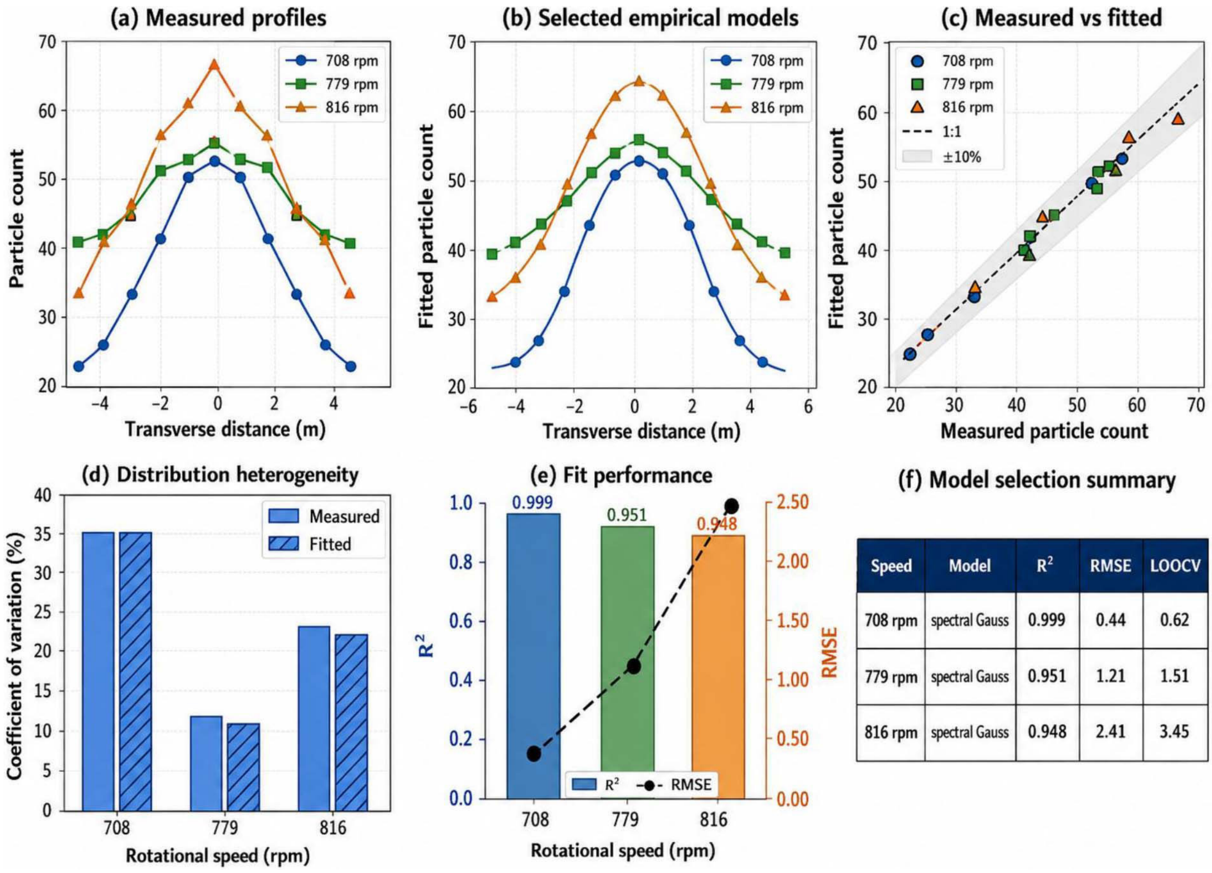

Figure 8. Effect of rotational speed on the spreading profile with the conical insert. Profiles measured at 708, 779, and 816 rpm and their fitted semi-empirical models

Table 3. Selected semi-empirical models for transverse spreading profiles

Configuration	Selected model	k	AICc	LOOCV RMSE	R2	RMSE	CV exp (%)
Without insert - 779 rpm	Background + central Gaussian	3	25.16	2.48	0.992	2.04	68.2
With insert - 708 rpm	Background + central Gaussian	3	-8.65	0.62	0.999	0.44	35.1
With insert - 779 rpm	Background + central Gaussian	3	13.56	1.51	0.951	1.21	12.0
With insert - 816 rpm	Background + central Gaussian	3	28.82	3.45	0.948	2.41	23.0

Linear models were retained for the three granulometric half-profiles (Table 4). Fit quality varied according to profile shape. The 1.00 mm class had the highest R2 among granulometric classes (0.878), while the 1.25 mm class had a lower R2 (0.457) because its profile was almost flat, leaving little variance to explain. The low RMSE of the 1.25 mm class (0.43 particles) nevertheless indicates that the fitted values remained close to the measured counts.

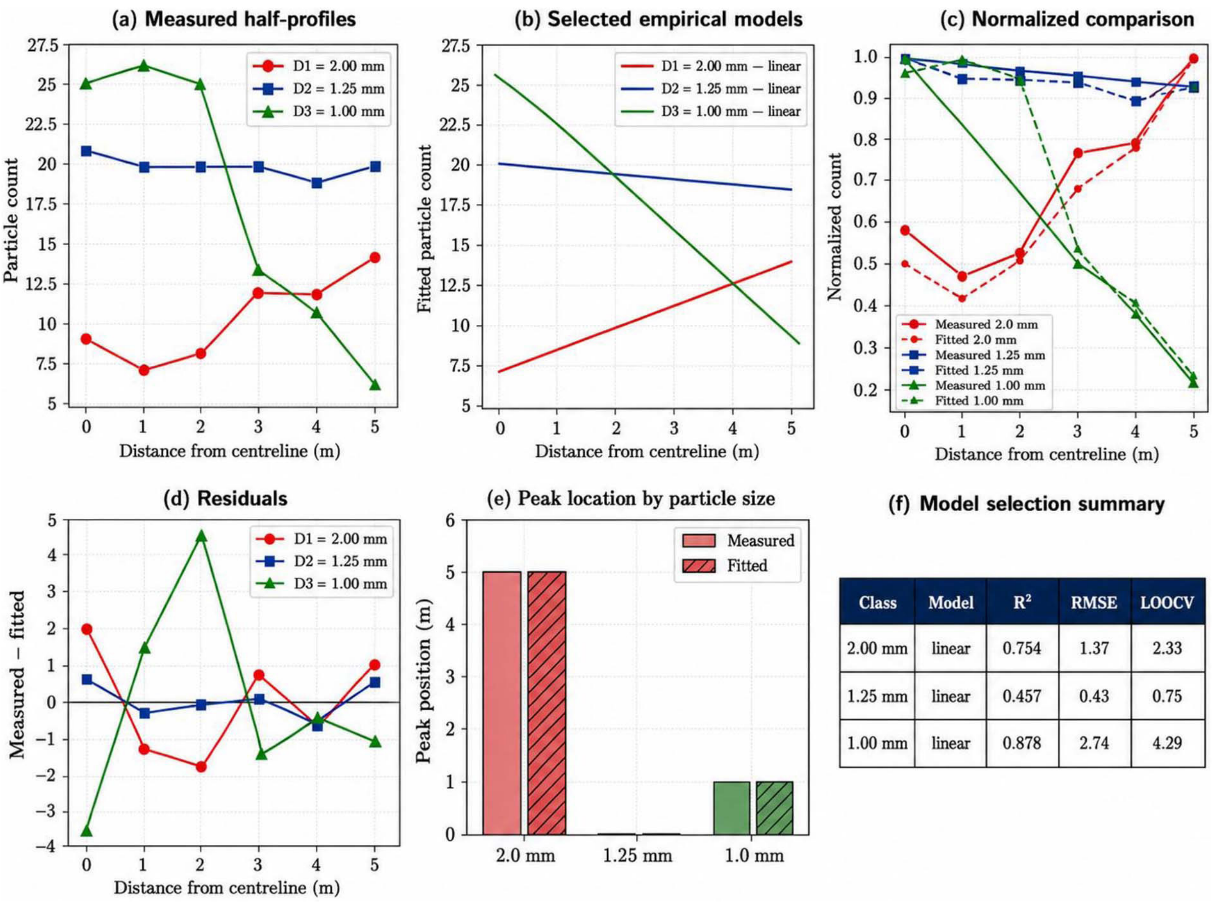

Figure 9. Effect of particle size on the half-profile measured at 779 rpm with the conical insert. Fitted profiles for D1, D2 and D3

Table 4. Selected semi-empirical models for granulometric half-profiles

Particle class	Selected model	k	AICc	LOOCV RMSE	R2	RMSE	CV exp (%)
D = 2.00 mm	Linear	2	11.74	2.33	0.754	1.37	28.7
D = 1.25 mm	Linear	2	-2.26	0.75	0.457	0.43	3.2
D = 1.00 mm	Linear	2	20.10	4.29	0.878	2.74	48.3

Note: Granulometric profiles were fitted independently because particle size affected the distribution shape.

Global model evaluation

The global evaluation confirmed that the semi-empirical approach provided strong descriptive performance for the transverse profiles and acceptable descriptive performance for the granulometric half-profiles (Figure 10). Across the four full transverse profiles, R2 values ranged from 0.948 to 0.999, and Willmott d values ranged from 0.987 to 1.000 (Table 5).

Granulometric fits were more variable because each half-profile contained only six measurement points and because the observed behaviors differed between particle-size classes. The 1.25 mm profile was nearly uniform, resulting in low explained variance but small absolute error. Therefore, R2 was interpreted together with RMSE, MAE, and Willmott d rather than as the sole measure of model performance.

To further support the reliability of the experimental results, descriptive statistics and statistical comparisons were calculated from the supplementary dataset. Mean values were complemented by standard deviation, standard error, and coefficient of variation. One-way ANOVA showed significant differences among the four transverse configurations for particle-count data, $F(3, 128) = 6.092$, $p = 6.581 \times 10^{-4}$. Similarly, ANOVA performed on the transect-level coefficient of variation showed significant differences in spatial heterogeneity among configurations, $F(3, 8) = 77.573$, $p = 2.962 \times 10^{-6}$. These results indicate that the observed differences among configurations were statistically supported and were not based only on mean particle-count profiles. The main statistical reliability indicators are summarized in Table 6, while the complete descriptive statistics, raw data, and calculation workflow are provided in Supplementary File S1.

To provide numerical evidence supporting the reliability and reproducibility of the results, the complete modeling and statistical outputs were provided in Supplementary File S1. This supplementary file includes raw experimental profiles, replicate-level support values, descriptive statistics, standard deviations, standard errors,

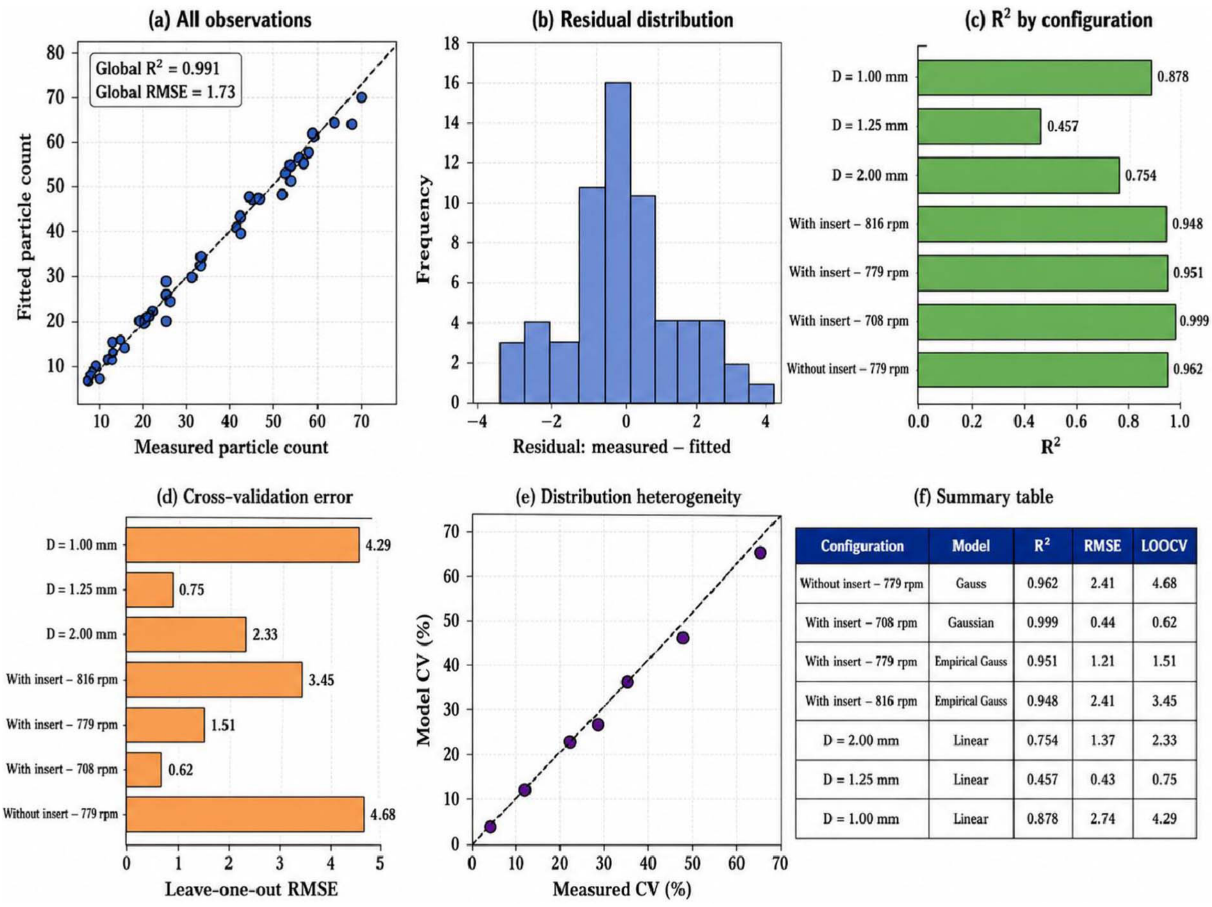

Figure 10. Global model evaluation. The figure summarizes measured-versus-predicted relationships, residuals, cross-validation error, and performance indicators

Table 5. Global summary of semi-empirical model performance

Configuration	Selected model	R2	RMSE	MAE	LOOCV RMSE	Willmott d	MAPE (%)
Without insert - 779 rpm	Background + Gaussian	0.992	2.04	1.76	2.48	0.998	8.3
With insert - 708 rpm	Background + Gaussian	0.999	0.44	0.38	0.62	1.000	1.1
With insert - 779 rpm	Background + Gaussian	0.951	1.21	1.05	1.51	0.987	2.2
With insert - 816 rpm	Background + Gaussian	0.948	2.41	2.28	3.45	0.987	4.7
D = 2.00 mm	Linear	0.754	1.37	1.27	2.33	0.925	13.8
D = 1.25 mm	Linear	0.457	0.43	0.37	0.75	0.771	1.9
D = 1.00 mm	Linear	0.878	2.74	2.23	4.29	0.967	12.3

Note: Table combines transverse profiles and granulometric half-profiles generated by the final semi-empirical workflow

coefficients of variation, fitted model parameters, full AICc comparisons among candidate models, leave-one-out cross-validation outputs, residual diagnostics where applicable, and calculation notes. In the main manuscript, only the most relevant reliability indicators are summarized to maintain readability, while the complete calculation workflow is provided in Supplementary File S1 for independent verification.

DISCUSSION

The results demonstrate that the conical insert substantially modified the transverse distribution pattern of the quarter-scale centrifugal spreader. The reference configuration without insert produced a highly concentrated central profile, whereas the insert configuration at 779 rpm generated a flatter profile with a much lower coefficient of variation. This suggests that the insert acted as a simple flow-guiding device that redistributed particles before their arrival on the rotating disc, reducing central accumulation and improving lateral deposition.

The improvement observed with the insert is consistent with the general principle that the initial position of particles on the disc strongly affects their ejection trajectory and the resulting transverse profile. By forcing part of the granular flow to follow longitudinal channels and a conical surface, the insert likely changed the initial radial distribution of particles on the disc before particle ejection. This mechanism is consistent with the fitted model parameters, which showed a reduction in profile amplitude (A) and an increase in baseline level (C) when the conical insert was used. These changes indicate lower central accumulation and a more homogeneous transverse redistribution of particles. This interpretation agrees with earlier modeling and experimental studies showing that feed position and cone-disc geometry influence spreading quality (Dintwa et al., 2004; Olieslagers et al., 1996).

Rotational speed had a clear effect under the insert configuration. The lowest CV was obtained at 779 rpm, while 708 and 816 rpm produced higher variability. This indicates that insert performance cannot be evaluated independently of disc speed. At lower speed, particle acceleration may be insufficient to redistribute the flow widely enough, whereas at higher speed the stronger ejection may increase local heterogeneity or amplify small differences in particle contact conditions. The tested intermediate speed, therefore represented the best compromise between lateral redistribution and profile regularity.

Table 6. Statistical reliability indicators derived from the supplementary raw dataset

Analysis	Response variable	Groups compared	F statistic	p-value
One-way ANOVA	Total particle count	4 transverse configurations	F(3, 128) = 6.092	6.581×10^{-4}
One-way ANOVA	Transect-level CV (%)	4 configurations	F(3, 8) = 77.573	2.962×10^{-6}

The granulometric analysis revealed that particle size was a major determinant of deposition pattern. The 1.25 mm fraction produced an almost uniform half-profile, while the 1.00 mm fraction was concentrated near the center, and the 2.00 mm fraction contributed more to distant positions. This behavior is consistent with differences in inertia, drag sensitivity, and contact stability on the disc. The low R2 obtained for the 1.25 mm class does not indicate poor practical agreement; instead, it reflects the low variance of an almost flat profile, as confirmed by the small RMSE and MAPE values. Rather, it reflects the limited variability of an almost uniform profile, for which traditional variance-based goodness-of-fit metrics become less informative. This interpretation is supported by the low RMSE and MAE values, which indicate that the absolute prediction errors remained limited despite the low R^2.

The modeling strategy was deliberately revised from a mechanistic physics-based model to a semi-empirical reduced-order model. This choice was scientifically important because the initial physical model did not sufficiently reproduce the experimental data. A full mechanistic simulation would require detailed information on particle-particle collisions, vane-particle impacts, stochastic rebounds, local disc roughness, air drag, and the instantaneous flow rate. These mechanisms were not measured in the present setup. The final semi-empirical model, therefore, provides a more transparent and defensible way to describe the measured profiles without overinterpreting the mechanical complexity of the prototype.

The study has several limitations. The experiments were conducted indoors using a quarter-scale prototype and particle counting rather than mass collection in standard trays. Although this procedure was justified by the small masses generated by the prototype and by the need to distinguish colored particle classes, field-scale confirmation would be required before direct extrapolation to commercial spreaders. In addition, scaling effects associated with the quarter-scale prototype may influence particle trajectories, particle-disc interactions, and airflow effects compared with full-scale field conditions. Future validation should therefore include full-scale tray-mass tests following ASABE S341, additional fertilizer products with contrasting granulometry and bulk density, and a wider range of flow rates and forward speeds. In addition, only one fertilizer type and a limited number of speeds were tested. The conclusions should therefore be interpreted as controlled laboratory evidence of the insert effect rather than as a universal field calibration for all fertilizer spreaders.

CONCLUSIONS

This study set out to evaluate whether a conical flow-guiding insert could improve the transverse distribution uniformity of a quarter-scale centrifugal fertilizer spreader, and to determine how rotational speed and particle size interact with this mechanical modification. This objective was achieved under the controlled indoor conditions tested.

The central hypothesis was supported: installing the conical insert immediately above the discharge zone reduced the coefficient of variation of the transverse profile from 68.2% without an insert to 12.0% with an insert at 779 rpm, confirming that redistributing the granular flow before disc contact produces a flatter and more uniform deposition pattern. The hypothesis that insert performance depends on rotational speed was also supported, with 779 rpm identified as the optimal speed among the three tested values, while 708 and 816 rpm produced higher variability. The hypothesis that particle size affects the spatial distribution pattern under the insert configuration was likewise supported: the 1.25 mm fraction produced the most uniform half-profile, the 1.00 mm fraction concentrated near the center, and the 2.00 mm fraction contributed more strongly to distant positions.

The main new finding of this work is that a simple, passive, low-cost upstream flow-guiding geometry can substantially improve fertilizer distribution uniformity without modifying the rotating disc, the vanes, or the motor system of the spreader. This addressed the gap previously identified in the literature, where the isolated mechanical contribution of a fixed conical insert at the hopper outlet had not been quantified separately from the combined effects of disc speed and particle diameter. The reduced-order semi-empirical model, selected through corrected Akaike information criterion and validated by leave-one-out cross-validation, provided a transparent and reproducible framework for comparing spreading configurations without requiring a full mechanistic simulation of particle motion.

These conclusions should be interpreted as controlled laboratory evidence obtained on a quarter-scale prototype using particle counting rather than standard tray-mass measurement. Future research should prioritize full-scale validation following ASABE S341 with tray-mass collection, testing of additional fertilizer products with contrasting granulometry and bulk density, and evaluation under a wider range of flow rates, forward speeds, and rotational speeds, in order to confirm whether the optimal speed and the magnitude of the uniformity gain observed here are transferable to commercial centrifugal spreaders.

Acknowledgements

The authors would like to thank the Department of Mechanical and Agro-Industrial Engineering, Higher School of Engineers of Medjez El Bab, University of Jendouba, for providing the experimental facilities used in this work.

REFERENCES

1. Antille, D. L., Gallar, L., Miller, P. C., Godwin, R. J. (2015). An investigation into the fertilizer particle dynamics off-the-disc. *Applied Engineering in Agriculture, 31*, 49–60. https://doi.org/10.13031/aea.31.10729
2. ASABE Standards. (2015). *Procedure for measuring distribution uniformity and calibrating granular broadcast spreaders (ASABE S341.5)*. American Society of Agricultural and Biological Engineers, St. Joseph, MI.
3. Burnham, K. P., Anderson, D. R. (2002). *Model selection and multimodel inference: A practical information-theoretic approach* (2nd ed.). Springer.
4. Cieniawska, B., Pentoś, K., Pieczarka, K. S., Kluza, P. A., Dereń, K., Surma, M., Jałoszyński, K. (2024). Optimisation of the fertilisation process for selected field spreaders. *Journal of Research and Applications in Agricultural Engineering, 69*(2), 48–56. https://doi.org/10.53502/jraae-200645
5. Coetzee, C., Lombard, S. (2011). Discrete element method modelling of a centrifugal fertiliser spreader. *Biosystems Engineering, 109*, 308–325. https://doi.org/10.1016/j.biosystemseng.2011.04.011
6. Dintwa, E., Van Liedekerke, P., Olieslagers, R., Tijskens, E., Ramon, H. (2004). Model for simulation of particle flow on a centrifugal fertiliser spreader. *Biosystems Engineering, 87*, 407–415. https://doi.org/10.1016/j.biosystemseng.2004.01.001
7. Guan, Z., Mu, S., Jiang, T., Li, H., Zhang, M., Wu, C., Jin, M. (2022). Development of centrifugal disc spreader on tracked combine harvester for rape undersowing rice based on DEM. *Agriculture, 12*(4), 562. https://doi.org/10.3390/agriculture12040562
8. Grift, T. E. (2000). Spread pattern analysis tool (SPAT): I. Development and theoretical examples. *Transactions of the ASAE, 43*(6), 1341–1350. https://doi.org/10.13031/2013.3031
9. Juodišius, G., Jotautienė, E., Mieldažys, R., Vaiciukevičius, E., Steponavičius, D., Bivainis, V. (2025). Investigation of granular organic fertilizer distribution uniformity in disk-type spreaders with standard and modified vane configurations. *Applied Sciences, 15*(24), 13076. https://doi.org/10.3390/app152413076
10. Khokhar, K. H., Demiraj, E., Lahori, A. H., Memon, M., Babar, H., Sethar, S., Panhwar, M. A., Kumar, M., Khokhar, Z. A., Afzal, A. (2025). Field experiment to evaluate the phosphate fertilizers effect on wheat' morphological traits. *Trends in Ecological and Indoor Environmental Engineering, 3*(4), 1–11. https://doi.org/10.62622/TEIEE.025.3.4.01-11
11. Kömekçi, F., Kömekçi, C., Doğu, D., Aykas, E. (2024). Effects of number of vanes, vane angle and disc peripheral speed on the distribution uniformity of twin-disc granular fertilizer broadcaster. *Heliyon, 10*(18), e37922. https://doi.org/10.1016/j.heliyon.2024.e37922
12. Kweon, G., Grift, T. E. (2006). Feed gate adaptation of a spinner spreader for uniformity control. *Biosystems Engineering, 95*, 19–34. https://doi.org/10.1016/j.biosystemseng.2006.05.003
13. Liedekerke, P. V., Tijskens, E., Dintwa, E., Anthonis, J., Ramon, H. (2006). A discrete element model for simulation of a spinning disc fertilizer spreader I. Single particle simulations. *Powder Technology, 170*, 71–85. https://doi.org/10.1016/j.powtec.2006.07.024
14. Liedekerke, P. V., Tijskens, E., Ramon, H. (2009). Discrete element simulations of the influence of fertiliser physical properties on the spread pattern from spinning disc spreaders. *Biosystems Engineering, 102*, 392–405. https://doi.org/10.1016/j.biosystemseng.2009.01.006
15. Liu, C., Song, J., Zhang, J., Du, X., Zhang, F. (2018). Design and performance experiment on centrifugal fertilizer spreader with a cone disc. *International Agricultural Engineering Journal, 27*, 44–52.
16. Lu, J., Shang, Q., Yang, Y., Li, Z., Li, J., Liu, Z. (2016). Performance analysis and experiment on granular fertilizer spreader with cone disc. *Transactions of the Chinese Society of Agricultural Engineering, 32*, 16–24. https://doi.org/10.11975/j.issn.1002-6819.2016.11.003
17. Nukeshev, S., Eskhozhin, D., Mamyrbayeva, I., Karaivanov, D., Gubasheva, A., Tleumbetov, K., Kossatbekova, D., Tanbayev, K. (2023). Mathematical modelling and designing of a universal

conical spreader for granular material. *Acta Technologica Agriculturae, 26*(3), 152–158. https://doi.org/10.2478/ata-2023-0020

18. Odiana, S., Godwin, O. G., Okoduwa, A. K. (2026). Integrating long-term climate trend analysis and household socioeconomic vulnerability to assess climate stress in the Niger Delta floodplain (Ughelli, Nigeria). *Trends in Ecological and Indoor Environmental Engineering, 4*(2), 12–21. https://doi.org/10.62622/TEIEE.026.4.2.12-21
19. Olieslagers, R., Ramon, H., Baerdemaeker, J. D. (1996). Calculation of fertilizer distribution patterns from a spinning disc spreader by means of a simulation model. *Journal of Agricultural Engineering Research, 63*, 137–152. https://doi.org/10.1006/jaer.1996.0016
20. Ou, M., Wang, G., Lu, Y., Zhang, Z., Pan, H., Jia, W., Dong, X. (2025). Structure optimization and performance simulation of a double-disc fertilizer spreader based on EDEM-CFD. *Agronomy, 15*(5), 1025. https://doi.org/10.3390/agronomy15051025
21. Patah, S. F. A., Othman, N. M. I. (2024). Influence of soil temperature on root development and microbial diversity in paddy fields: A comprehensive review. *Trends in Ecological and Indoor Environmental Engineering, 2*(4), 1–9. https://doi.org/10.62622/TEIEE.024.2.4.01-09
22. Sikder, A., Mumit, S. H. (2024). Investigation of the effectiveness of using *Luffa cylindrica* to reduce water consumption in agriculture. *Trends in Ecological and Indoor Environmental Engineering, 2*(4), 18–27. https://doi.org/10.62622/TEIEE.024.2.4.18-27
23. Villette, S., Cointault, F., Piron, E., Chopinet, B. (2005). Centrifugal spreading: An analytical model for the motion of fertiliser particles on a spinning disc. *Biosystems Engineering, 92*, 157–164. https://doi.org/10.1016/j.biosystemseng.2005.06.013
24. Villette, S., Piron, E., Miclet, D. (2017). Hybrid centrifugal spreading model to study the fertiliser spatial distribution and its assessment using the transverse coefficient of variation. *Computers and Electronics in Agriculture, 137*, 115–129. https://doi.org/10.1016/j.compag.2017.03.023
25. Willmott, C.J. (1982). Some comments on the evaluation of model performance. *Bulletin of the American Meteorological Society*, 63, 1309-1313. https://doi.org/10.1175/1520-0477(1982)063
26. Wuyep, S. Z. (2024). Effects of fire on physical and chemical properties of soil in Fwangnin Bokkos District, Nigeria. *Trends in Ecological and Indoor Environmental Engineering, 2*(3), 42–49. https://doi.org/10.62622/TEIEE.024.2.3.42-49
27. Wuyep, S. Z., Ogbole, A. S., James, W. (2026). Precipitation effectiveness and rice yield: Implications for agroecosystem resilience in Langtang South, Nigeria. *Trends in Ecological and Indoor Environmental Engineering, 4*(2), 35–43. https://doi.org/10.62622/TEIEE.026.4.2.35-43
28. Yildirim, Y., Kara, M. (2003). Effect of vane height on distribution uniformity in rotary fertilizer spreaders with different flow rates. *Applied Engineering in Agriculture, 19*, 691–696. https://doi.org/10.13031/2013.12730